Development 137, 1669-1677 (2010) doi:10.1242/dev.045823

Symmetry breaking and polarization of the *C. elegans* zygote by the polarity protein PAR-2

Seth Zonies, Fumio Motegi, Yingsong Hao and Geraldine Seydoux*

SUMMARY

Polarization of the *C. elegans* zygote is initiated by ECT-2-dependent cortical flows, which mobilize the anterior PAR proteins (PAR-3, PAR-6 and PKC-3) away from the future posterior end of the embryo marked by the sperm centrosome. Here, we demonstrate the existence of a second, parallel and redundant pathway that can polarize the zygote in the absence of ECT-2-dependent cortical flows. This second pathway depends on the polarity protein PAR-2. We show that PAR-2 localizes to the cortex nearest the sperm centrosome even in the absence of cortical flows. Once on the cortex, PAR-2 antagonizes PAR-3-dependent recruitment of myosin, creating myosin flows that transport the anterior PAR complex away from PAR-2 in a positive-feedback loop. We propose that polarity in the *C. elegans* zygote is initiated by redundant ECT-2- and PAR-2-dependent mechanisms that lower PAR-3 levels locally, triggering a positive-feedback loop that polarizes the entire cortex.

KEY WORDS: *Caenorhabditis elegans*, PAR proteins, PAR-2, Polarity

INTRODUCTION

Cell polarity is essential for the generation of cellular diversity in development and for the functioning of most differentiated cells. Polarity in many cell types depends on a group of conserved polarity regulators, collectively known as the PAR proteins. In polarized cells, several of the PAR proteins localize asymmetrically to specific cortical domains at the cell periphery. The formation of asymmetric PAR domains is thought to be a key step in cell polarization, but the mechanisms involved are not fully understood (Goldstein and Macara, 2007).

The *C. elegans* zygote is a classic model for the study of cell polarity (Kemphues, 2000). The zygote is an ovoid cell that becomes polarized along its long axis by the sperm-donated centrosome, which defines the posterior end. One advantage of the *C. elegans* zygote as a polarity model is that the entire polarization process can be visualized in real time, from the initial symmetry-breaking event to the first asymmetric division (17 minutes). Genetic and cellular analyses have led to a simple working model for how PAR domains are established in the *C. elegans* zygote (Munro and Bowerman, 2009). Before polarization, the PDZ domain proteins PAR-3 and PAR-6, and the kinase PKC-3, are uniformly distributed throughout the cortex. The kinase PAR-1 and the RING-finger protein PAR-2 are, by contrast, in the cytoplasm. PAR-2 is kept off the cortex by direct phosphorylation by the kinase PKC-3 (Hao et al., 2006). PAR-1 is also likely to be a PKC-3 substrate because PAR-1 has a conserved PKC site that is phosphorylated in the mammalian PAR-1 ortholog by aPKC, the mammalian PKC-3 ortholog (Hurov et al., 2004). Immediately before polarization at the end of the meiotic divisions, the cortex becomes highly dynamic, with actomyosin-rich cables contracting and relaxing throughout the length of the zygote (Munro et al., 2004). As the pronuclei form, the sperm nucleus and its associated centrosome move near the cortex. Contractions immediately cease in that area, causing the actomyosin network to collapse in a cortical flow that transports PAR-6 (and presumably PAR-3 and PKC-3 – the 'anterior' PARs) away from the centrosome, leaving PAR-1 and PAR-2 (the 'posterior' PARs) free to load on the posterior cortex (Munro et al., 2004).

How the sperm centrosome triggers cortical flow is not known, but it has been proposed that a key event is local inactivation of Rho (Jenkins et al., 2006; Motegi and Sugimoto, 2006; Schonegg and Hyman, 2006). The guanine nucleotide-exchange factor (GEF) for the small GTPase Rho, ECT-2, is required for the formation of the actomyosin-rich cables that tension the cortex (Motegi and Sugimoto, 2006; Schonegg and Hyman, 2006). Initially, ECT-2 is uniformly distributed, but then disappears from the area of the cortex nearest the sperm centrosome. This local disappearance of ECT-2 occurs even in the absence of Rho and the PAR proteins, suggesting that this is the event that inactivates Rho and initiates cortical flow (Motegi and Sugimoto, 2006). The sperm-enriched Rho GTPase-activating protein (GAP) CYK-4 may also contribute to local inactivation of Rho (Jenkins et al., 2006).

The anterior PARs are not required to initiate cortical flow but are required to amplify the flow in a positive-feedback loop (Cheeks et al., 2004; Munro et al., 2004), ensuring their rapid and complete mobilization away from the posterior half of the cortex. PAR-2 is also not required to initiate flow or PAR asymmetry (Cheeks et al., 2004; Cuenca et al., 2003; Munro et al., 2004). PAR-2 is required, however, to prevent a reverse flow later during mitosis, which would otherwise sweep myosin and the anterior PARs back into the posterior cortex (Cuenca et al., 2003; Munro et al., 2004). These observations have suggested that PAR-2 is only a passive player during initiation and functions primarily in polarity maintenance (Cheeks et al., 2004; Cuenca et al., 2003; Munro et al., 2004).

A prediction of the cortical flow model is that without myosin contractility, the anterior PARs should remain uniformly distributed at the cortex and PAR-2 should remain in the cytoplasm. Consistent with this prediction, RNA interference (RNAi)-mediated depletion of the myosin regulatory light chain MLC-4 eliminates cortical flows and has been reported to block PAR-3 polarization in zygotes before pronuclear meeting (Shelton et al., 1999). Unexpectedly,

Department of Molecular Biology and Genetics, Howard Hughes Medical Institute, Center for Cell Dynamics, Johns Hopkins School of Medicine, 725 N. Wolfe Street, PCTB 706, Baltimore, MD 21205, USA.

*Author for correspondence (gseydoux@jhmi.edu)

Accepted 1 March 2010

however, PAR-2 still loads on the cortex near the sperm centrosome in *mlc-4(RNAi)* zygotes (Shelton et al., 1999). This observation raises the possibility that mechanisms other than ECT-2-dependent flows contribute to polarity initiation and place PAR-2 on the posterior cortex.

In this study, we investigate this possibility further using a temperature-sensitive *ect-2* allele that eliminates ECT-2-dependent early cortical flows. We show that under these conditions, PAR-2 can break symmetry and polarize the entire zygote, revealing a second pathway for polarity initiation.

MATERIALS AND METHODS

Strains and genetics

Nematodes were cultured as described (Brenner, 1974). All strains (Table 1) were maintained at 20°C.

ax751 was identified as follows. A collection of ~800 temperature-sensitive embryonic lethal mutants (M. R. Wallenfang and G.S., unpublished) was raised for 16 hours at 25°C and immunostained with a monoclonal anti-PIE-1 antibody (Tenenhaus et al., 1998). Twenty-three mutants that mislocalize PIE-1 were recovered, including *ax751*. The mutants were outcrossed once to JH227 (PIE-1::GFP transgene) and *ax751* was outcrossed five more times against N2 (wild type). Single nucleotide polymorphism (SNP) mapping was performed as described (Davis et al., 2005) to map *ax751* to chromosome II. Complementation testing and sequencing of genomic DNA demonstrated that *ax751* is an allele of the previously characterized gene *ect-2* (Morita et al., 2005). The viability counts in Fig. 1 were performed by shifting L4 hermaphrodites grown at 20°C to 15°C or 25°C for 24 hours, then transferring to a clean plate for 8 hours (two mothers per plate), removing the mothers and counting the embryos laid. Hatched worms were counted the following day.

RNAi

T19E10.1(*ect-2*), F58B6.3(*par-2*) and F58A4.4(*pri-1*) were obtained from the RNAi feeding library of Ahringer and colleagues (Kamath et al., 2003). All RNAi experiments were performed using the feeding method (Timmons and Fire, 1998). Bacterial cultures for feeding were grown overnight on nematode nutritional growth medium plates containing 50 μg/ml carbenicillin and 1 mM IPTG. L4 hermaphrodites were allowed to feed for 24 hours at 25°C before examination, or for 30 hours in the case of *ect-2(RNAi)*.

In the case of the *par-2/par-3* epistasis experiments and the *mlc-4(RNAi)* experiments, the mothers were also soaked in double-stranded RNA (dsRNA) for 24 hours before feeding on the RNAi bacteria. Soaking was performed by incubating mothers in 0.8-1.0 μg/μl dsRNA at 20°C for 24 hours before transferring to the feeding plates for 24 hours at 25°C (Maeda et al., 2001).

Imaging

All movies were performed at 25°C. Hermaphrodites were shifted from 20°C to 25°C as L4 for 24 hours, dissected in M9 on coverslips, inverted onto 3% agarose pads and sealed with Vaseline. Embryos were viewed with a 63× Plan-Apochromat 1.4 NA oil-immersion lens using a CSUX-A1 spinning-disc confocal system (Yokogawa Electric) mounted on a Zeiss imager Z1. The specimens were illuminated with a Laser Stack containing 491 and 561 solid-state diode lasers (Intelligent Imaging Innovations). Images were acquired with a Cascade QuantEM:512 SC camera (Photometrics) controlled by SlideBook software (Intelligent Imaging Innovations). Image processing was performed with Photoshop (Adobe Systems).

Cortical NMY-2::GFP and mCherry::PAR-2 images, representing a single, in-focus cortical section, were acquired every 5 seconds. Exposures were 60 milliseconds and 1 second, respectively. Pronuclear meeting was determined by briefly shifting the focus down, during a time-lapse capture, to show a transverse section of the zygote as pronuclei met. Flickering in movies is a result of this change in focal planes.

Cross-sectional GFP::PAR-2 and mCherry::PAR-6 images were also acquired every 5 seconds. Exposures were 100 milliseconds and 300 milliseconds, respectively.

For kymograph analysis, a line was drawn along the long axis of the zygote and the Smooth-curve analysis tool in SlideBook was used to generate the kymograph. Pixel width was set to two.

Changes in average cortical NMY-2::GFP levels were quantified as follows. The cortex was divided into anterior and posterior halves. Average fluorescence was measured in each region 3 minutes before pronuclear meeting (pronuclear migration) and at the point when maximum average fluorescence intensity was reached, corresponding to nuclear envelope breakdown (NEBD). Fluorescence intensity from a region selected outside the zygote was subtracted from each region to correct for background. Fold increase was calculated as $Avg_{NEBD}/Avg_{pro\text{-}mig}$ where pro-mig is pronuclear migration. Five zygotes were analyzed for each genotype, except for *mlc-4(RNAi)* where n=3. Error bars indicate ± s.e.m.

Pronuclear formation was defined as the time at which the paternal pronucleus reached 3 μm in diameter, as determined using cross-sectional time-lapse imaging. NEBD was defined as the first time frame in which the fusion under study was no longer excluded from pronuclei. Polarity was defined as the first time frame in which the fusion under study became asymmetrically distributed.

Immunostaining

Hermaphrodites raised at 25°C for 24 hours were frozen between a slide and coverslip on a dry ice-cooled aluminium block, and then fixed on the slide without coverslip in methanol:acetone at –20°C (Shaham, 2006). For phospho-myosin regulatory light chain staining, samples were fixed in 4% paraformaldehyde in PBS for 15 minutes. Antibodies and dilutions were as

Table 1. Strains used in this study

Name	Description	Genotype
JH2754	*ect-2(ax751)* with no transgene	*ect-2(ax751) II*
VC114*	Balanced *ect-2(gk44)*	*T19E10.1a(gk44)/mIn1[mIs14 dpy-10(e128)] II*
JH227	*pie-1 promoter*:PIE-1::GFP:*pie-1 3′UTR*	*axEx73[pJH3.92]*
JH1536	PIE-1::GFP in *ect-2(ax751)*	*ect-2(ax751) II; axEx73[pJH3.92]*
JJ1473*	*nmy-2 promoter*:NMY-2::GFP:*nmy-2 3′UTR*	*unc-119; zuIs45[nmy-2::gfp] V*
JH2652	NMY-2::GFP in *ect-2(ax751)*	*ect-2(ax751) II; zuIs45[nmy-2::gfp] V*
JH2647	mCherry::PAR-6;GFP::PAR-2	*axIs1928[pEG66]; axIs1182[pYH2.31]*
JH2657	mCherry::PAR-6;GFP::PAR-2 in *ect-2(ax751)*	*ect-2(ax751) II; axIs1928[pEG66]; axIs1182[pYH2.31]*
JH2761	NMY-2::GFP in *par-3(it71)*	*par-3(it71) unc-32/qc1 III; zuIs45[nmy-2::gfp] V*
JH2756	NMY-2::GFP in *ect-2(ax751);par-3(it71)*	*ect-2(ax751) II; par-3(it71) unc-32/qc1 III; zuIs45[nmy-2::gfp] V*
JH2755	*ect-2(ax751);par-1(it51)*	*ect-2(ax751) II; rol-4(sc8) par-1(it51) VInT1[qIS51] (IV;V)*
JH2759	NMY-2::GFP;mCherry::PAR-2	*axIs1929[pFM033]; zuIs45[nmy-2::gfp] V*
JH2757	NMY-2::GFP;mCherry::PAR-2 in *ect-2(ax751)*	*ect-2(ax751) II; axIs1929[pFM033]; zuIs45[nmy-2:gfp] V*
JH2648	*pie-1 promoter*:mCherry::PAR-6:*pie-1 3′UTR*	*unc-119; axIs1928[pEG66]*
JH2656	mcherry::PAR-6 in *ect-2(ax751)*	*ect-2(ax751) II; axIs1928[pEG66]*
JH2654	GFP::PAR-2 in *ect-2(ax751)*	*ect-2(ax751) II; axIs1182[pYH2.31]*

*All strains were generated in this study except VC114 [The Caenorhabditis Genetics Center (CGC)] and JJ1473 (Nance et al., 2003).

follows: 1:50 rabbit anti-PAR-2 (Gotta et al., 2003), 1:30 mouse anti-PAR-3 P4A1 monoclonal (Nance et al., 2003), 1:400 rabbit anti-GFP (Invitrogen a11122) and 1:50 rabbit anti-phospho-myosin regulatory light chain (MLC2) (Cell Signaling #3671). All antibodies were visualized with FITC-conjugated secondary antibodies except PAR-3, which was visualized by a Cy3-conjugated antibody. Images of immunostained embryos were captured by epifluorescence. Phospho-myosin regulatory light chain-immunostained embryos were captured by the spinning disc confocal system described above. For confirmation of the specificity of the anti-phospho-myosin regulatory light chain antibody, see Fig. S1 in the supplementary material.

RESULTS

ax751 is a hypomorphic allele of *ect-2*

We identified *ax751* in a screen for temperature-sensitive embryonic lethal mutations that mislocalize PIE-1, a maternal protein that segregates to the posterior of the zygote (Fig. 1; see Materials and methods). Mapping, complementation testing and sequencing showed that *ax751* is a missense mutation in *ect-2*. *ect-2* codes for a GEF for the small Rho family GTPase RHO-1 (Morita et al., 2005). *ax751* replaces a glycine with an arginine at position 738, which is a conserved residue among nematode ECT-2 proteins (Fig. 1A). Hermaphrodites homozygous for a deletion in *ect-2* [*ect-2(gk44)*] are sterile (see www.celeganskoconsortium.omrf.org). Hermaphrodites homozygous for *ect-2(ax751)* are fertile, but their embryos exhibit temperature-sensitive lethality. *ect-2(ax751)* mothers raised at 15°C laid 85% viable embryos, and mothers shifted to 25°C as L4 larvae laid only 10% viable embryos (Fig. 1B). *ect-2(ax751)/ect-2(gk44)* mothers laid even fewer viable embryos (Fig. 1B), consistent with *ect-2(ax751)* being a hypomorphic allele. At 25°C, embryos from *ect-2(ax751)* hermaphrodites exhibited the same range of phenotypes (see below) as embryos derived from mothers depleted for *ect-2* by RNAi, with one exception: whereas *ect-2(RNAi)* zygotes never complete the first cleavage (Dechant and Glotzer, 2003), *ect-2(ax751)* zygotes undergo a normal first cleavage in utero and exhibit cleavage defects only in later divisions (data not shown). First-cleavage defects, however, were sometimes seen in *ect-2(ax751)* zygotes imaged under a coverslip. Taken together, these observations suggest that *ect-2(ax751)* is a hypomorphic allele that retains partial *ect-2* function.

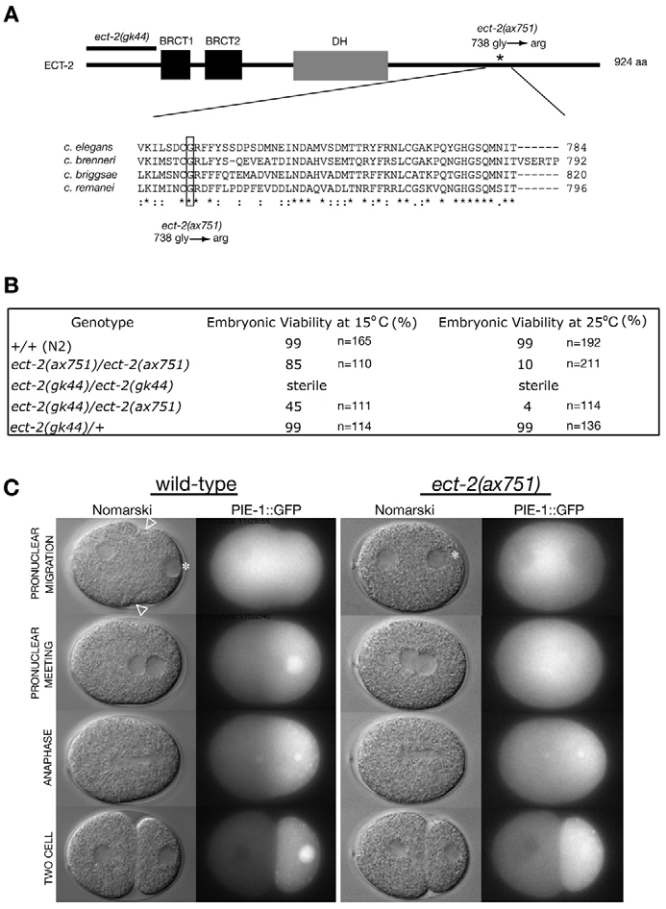

Genotype	Embryonic Viability at 15°C (%)		Embryonic Viability at 25°C (%)	
+/+ (N2)	99	n=165	99	n=192
ect-2(ax751)/ect-2(ax751)	85	n=110	10	n=211
ect-2(gk44)/ect-2(gk44)	sterile		sterile	
ect-2(gk44)/ect-2(ax751)	45	n=111	4	n=114
ect-2(gk44)/+	99	n=114	99	n=136

Fig. 1. *ax751* is a hypomorphic allele of *ect-2*. (**A**) Schematic of *C. elegans* ECT-2, showing its functional domains and the location of *ect-2(gk44)* and *ect-2(ax751)*. *gk44* is a deletion that removes sequence from –33 to +450 bp, relative to the ATG. Glycine 738 is conserved among nematodes, as shown in the Clustal W alignment of ECT-2 beneath. (**B**) Complementation testing of *ect-2(ax751)* with *ect-2(gk44)* demonstrating that *ax751* is a hypomorphic allele of *ect-2*. (**C**) Nomarski and fluorescence time-lapse images of wild-type and *ect-2(ax751)* zygotes expressing PIE-1::GFP. Arrowheads indicate cortical ruffling. Asterisk indicates paternal pronucleus. PIE-1::GFP segregates before pronuclear meeting in wild-type zygotes, but segregates after pronuclear meeting in *ect-2(ax751)* zygotes. In this and subsequent figures, zygotes are oriented with the anterior pole to the left. *C. elegans* zygotes are ~50 μm in length.

Polarization dynamics are disrupted in *ax751* zygotes

ect-2 is required for the formation of the actomyosin cables that tension the cortex of the zygote during polarization (Motegi and Sugimoto, 2006; Schonegg and Hyman, 2006). As expected, we found that *ax751* zygotes do not exhibit cortical ruffling (Fig. 1C). *ax751* zygotes segregated PIE-1 later than wild-type zygotes and underwent an asymmetric first cleavage, indicating that polarization, although delayed, does eventually occur in this background (Fig. 1C).

To examine cortical polarity directly, we created a line co-expressing NMY-2::GFP and mCherry::PAR-2 and imaged cortical sections. In wild-type zygotes, NMY-2::GFP assembles in a dynamic network of thick cables that segregates asymmetrically to the anterior during pronuclear migration (‘early wave’, Fig. 2A,D; see Movie 1 in the supplementary material). After pronuclear meeting, the cables disassemble and are replaced by a fine meshwork of small foci, retaining a higher density in the anterior (Fig. 2A,D; see Movie 1 in the supplementary material) (Munro et al., 2004). In *ax751* zygotes, NMY-2::GFP did not assemble in cables and remained in small foci throughout the first cell cycle (Fig. 2A; see Movie 2 in the supplementary material), as reported previously for *ect-2(RNAi)* (Motegi and Sugimoto, 2006; Schonegg and Hyman, 2006). After pronuclear meeting, however, the density of cortical NMY-2::GFP foci increased and a posterior-to-anterior wave (‘late wave’) formed a NMY-2::GFP high-abundance domain in the anterior and a NMY-2::GFP low-abundance domain in the posterior (Fig. 2A,D; see Movie 2 in the supplementary material). The late wave was also observed in *ect-2(RNAi)* zygotes, which do not undergo cleavage (5/5) (Fig. 2D; see Movie 3 in the supplementary material) (Schonegg and Hyman, 2006).

In wild-type zygotes, mCherry::PAR-2 loads on the posterior cortex coincident with the formation of strong anterior NMY-2::GFP flows (early wave; 7/7) (Fig. 2D; see Movie 1 in the supplementary material) (Munro et al., 2004). In *ect-2(ax751)*, mCherry::PAR-2 loaded before the late NMY-2::GFP wave (6/6) (Fig. 2D; see Movie

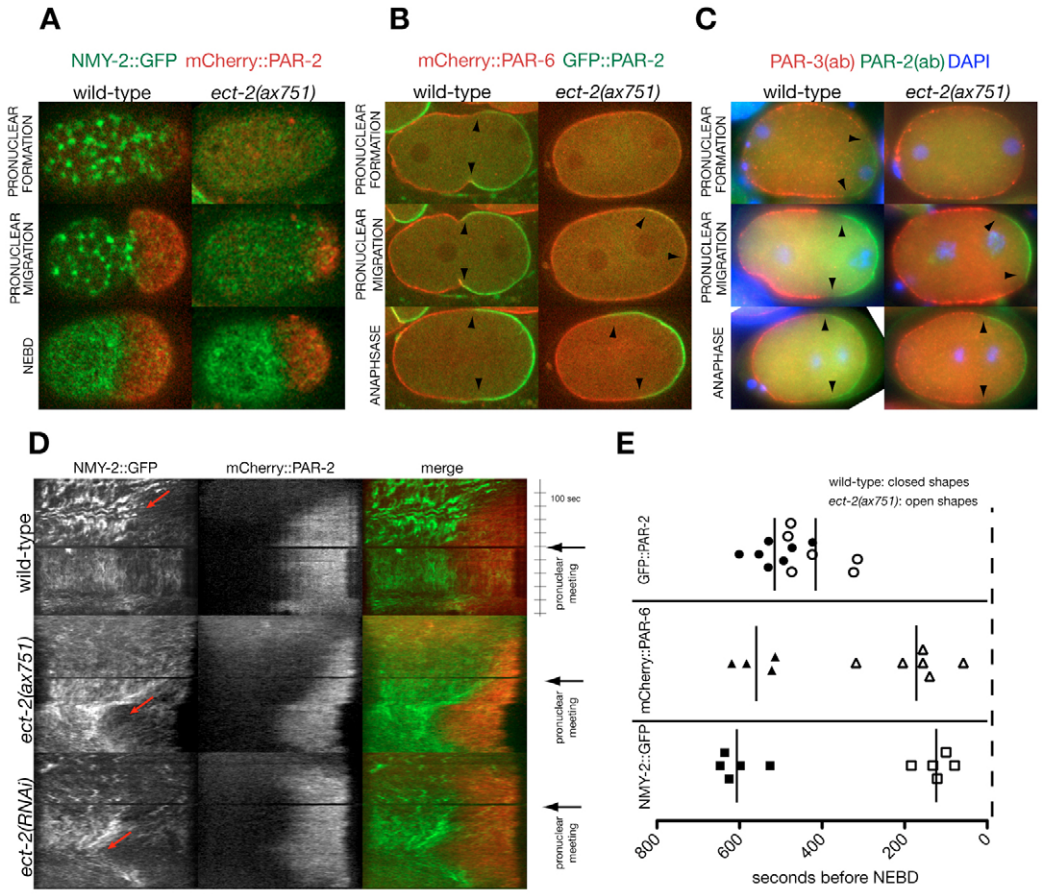

Fig. 2. Polarization dynamics are disrupted in *ax751* zygotes. (**A**) Time-lapse confocal images of cortical sections of wild-type and *ect-2(ax751) C. elegans* zygotes co-expressing NMY-2::GFP and mCherry::PAR-2. Large contractile filaments of NMY-2::GFP are visible in wild-type but absent from *ect-2(ax751)* zygotes. By nuclear envelope breakdown (NEBD), *ect-2(ax751)* zygotes have formed a dense asymmetric network of myosin and PAR-2 has loaded on the posterior cortex (see Movies 1 and 2 in the supplementary material). (**B**) Time lapse confocal images of transverse sections of wild-type and *ect-2(ax751)* zygotes co-expressing mCherry::PAR-6 and GFP::PAR-2. Arrowheads indicate the extent of the GFP::PAR-2 domain, which initially overlaps with that of mCherry::PAR-6 in *ect-2(ax751)* zygotes (see Movies 4 and 5 in the supplementary material). (**C**) Co-staining of PAR-2 and PAR-3 in wild-type and *ect-2(ax751)* zygotes that express no transgenes. The PAR-2 domain in *ect-2(ax751)* (arrowheads) is initially smaller than in wild type, but catches up by mitosis (anaphase). (**D**) Kymographs of cortical sections of wild-type, *ect-2(ax751)* and *ect-2(RNAi)* zygotes co-expressing NMY-2::GFP and mCherry::PAR-2. The vertical axis represents time. Cortical flows appear as diagonal lines on the kymographs (red arrows). Note that prominent cortical flows arise before pronuclear meeting in wild-type zygotes and after pronuclear meeting in *ect-2(ax751)* and *ect-2(RNAi)* zygotes (see Movies 1-3 in the supplementary material). (**E**) Polarization timing in wild-type (closed symbols) compared with *ect-2(ax751)* (open symbols) zygotes. Each data point represents one embryo filmed from pronuclear formation to NEBD. Time of polarization was scored as the earliest time at which asymmetry could be detected in the time-lapse movie. Vertical bars represent averages for each group. In wild-type zygotes, GFP::PAR-2, mCherry::PAR-6 and NMY-2::GFP asymmetries all arise early on (at least 400 seconds before NEBD). In *ect-2(ax751)* zygotes, asymmetries are delayed, with GFP::PAR-2 asymmetry appearing first, followed an average of 317 seconds later by mCherry::PAR-6 and NMY-2::GFP asymmetries.

2 in the supplementary material). When the NMY-2::GFP wave initiated, the mCherry::PAR-2 domain expanded behind the receding NMY-2::GFP high-abundance domain (Fig. 2D).

Consistent with PAR-2 loading before the NMY-2::GFP wave in *ect-2(ax751)*, we found that in *ect-2(ax751)* zygotes co-expressing mCherry::PAR-6 and GFP::PAR-2, GFP::PAR-2 overlapped with mCherry::PAR-6 for an average of 251±36 seconds before mCherry::PAR-6 receded towards the anterior (Fig. 2B,E). This observation is consistent with that of Schonegg and Hyman (Schonegg and Hyman, 2006), who reported an overlap between GFP::PAR-2 and endogenous PAR-6 in *ect-2(RNAi)* zygotes. As with NMY-2::GFP, segregation of mCherry::PAR-6 was delayed, occurring only after pronuclear meeting in most (4/6) *ect-2(ax751)* zygotes examined (Fig. 2B,E; see Movies 4 and 5 in the supplementary material).

To examine the distribution of endogenous PAR proteins, we co-stained wild-type and *ect-2(ax751)* zygotes that express no transgenes with anti-PAR-3 and anti-PAR-2 antibodies. We focused on PAR-3 and PAR-2 because they are essential to localize the other PAR proteins to their respective domains [PAR-3 is essential to localize PAR-6 and PKC-3 in the anterior cortex, and PAR-2 is essential to localize PAR-1 in the posterior cortex (Guo and Kemphues, 1996)]. Wild-type zygotes formed non-overlapping PAR-2 and PAR-3 domains from pronuclear formation onwards (9/9) (Fig. 2C). *ect-2(ax751)* zygotes formed posterior PAR-2 domains during pronuclear migration but these domains were smaller than in the wild type until mitosis (9/9) (Fig. 2C). Most (6/9) *ect-2(ax751)* zygotes also segregated PAR-3 (Fig. 2C), but in a minority of zygotes (3/9) low levels of PAR-3 could still be detected on the posterior cortex overlapping with PAR-2 (see Fig. S2 in the

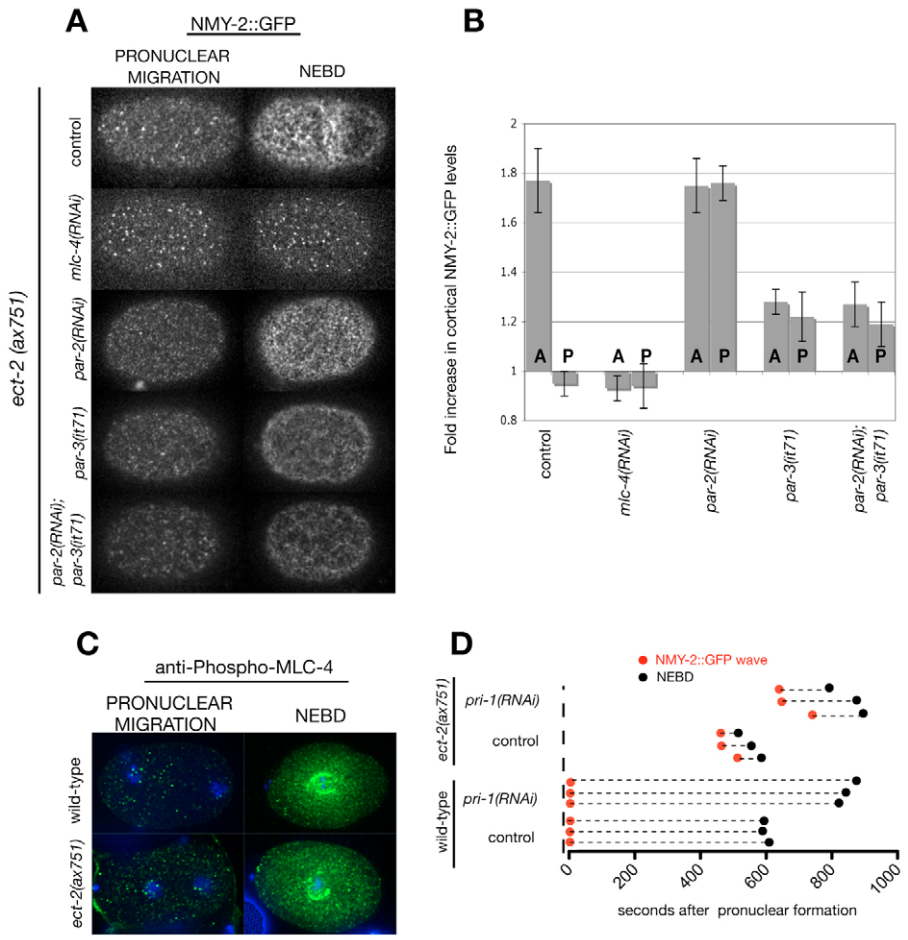

Fig. 3. PAR-2 and PAR-3 regulate myosin dynamics in *ect-2(ax751)* zygotes. (**A**) Time-lapse confocal images of cortical sections of *ect-2(ax751) C. elegans* zygotes expressing NMY-2::GFP and treated with the indicated RNAi. The same zygotes are shown at two stages: during pronuclear migration and at NEBD. During this time, NMY-2::GFP levels increase in the anterior cortex in the control and throughout the whole cortex in *par-2(RNAi)* zygotes and this increase is dependent on PAR-3 (see Movies 2 and 6-8 in the supplementary material). (**B**) Quantification of cortical NMY-2::GFP. The fold increase in cortical NMY-2::GFP was calculated by comparing fluorescence intensities in the cortex of live zygotes imaged during pronuclear migration and again during NEBD (see Materials and methods). (**C**) Immunostaining of phospho-MLC-4 (green) in wild-type and *ect-2(ax751)* zygotes that express no transgenes. DNA staining is with DAPI (blue). (**D**) Timing of the NMY-2::GFP wave in *pri-1(RNAi)* and control zygotes. Each line represents one embryo filmed from pronuclear meeting to NEBD. Red dots denote the timing of the NMY-2::GFP wave, and black dots denote the timing of NEBD relative to pronuclear formation.

supplementary material). Staining with anti-PAR-3 alone confirmed these results: 2/6 *ect-2(ax751)* zygotes before pronuclear meeting had PAR-3 throughout the cortex compared with 0/6 wild-type zygotes (data not shown).

We conclude that in *ect-2(ax751)* zygotes, strong myosin flows do not develop during pronuclear migration. During that time, PAR segregation is inefficient, with PAR-2 loading on the posterior cortex before complete clearing of the anterior PARs. After pronuclear meeting, strong myosin flows form (late wave) and the anterior and posterior PAR domains contract and expand, respectively, to reach wild-type sizes and no longer overlap.

The late myosin wave in *ect-2(ax751)* zygotes correlates with increased cortical NMY-2 and with MLC-4 phosphorylation and cell cycle progression

We noticed that the onset of the myosin wave in *ect-2(ax751)* zygotes was accompanied by an increase in NMY-2::GFP on the cortex (Fig. 2A,D; see Movie 2 in the supplementary material). Cortical NMY-2::GFP fluorescence increased by 1.8-fold from pronuclear meeting to nuclear envelope breakdown (NEBD; ~3 minutes after pronuclear meeting) (Fig. 3A,B). Myosin 2 interaction with cortical actin is regulated by the myosin regulatory light chain encoded by *mlc-4* in nematodes (Riento and Ridley, 2003). As expected, depletion of *mlc-4* by RNAi in *ect-2(ax751)* zygotes blocked the wave and the increase in cortical NMY-2::GFP (Fig. 3A,B). MLC-4 is activated by phosphorylation (Ikebe and Hartshorne, 1985). Using an antibody specific for phosphorylated MLC-4 (P-MLC-4) (see Fig. S1 in the supplementary material), we found that P-MLC-4 levels increase dramatically at pronuclear meeting and are kept high throughout NEBD in both wild-type and *ect-2(ax751)* zygotes (Fig. 3C).

To determine whether the NMY-2 wave in *ect-2(ax751)* zygotes is linked to cell cycle progression, we delayed the cell cycle by reducing the DNA polymerase primase subunit *pri-1* by RNAi (Encalada et al., 2000). *pri-1(RNAi)* delayed NEBD by ~250 seconds in wild-type and *ect-2(ax751)* zygotes. *pri-1(RNAi)* had no effect on NMY-2::GFP in wild-type zygotes, but delayed the NMY-2::GFP wave by ~200 seconds in *ect-2(ax751)* zygotes (Fig. 3D). These results suggest that, unlike in wild type, the myosin wave in *ect-2(ax751)* zygotes is dependent on a cell cycle-regulated event, perhaps linked to MLC-4 activation.

Myosin flows in *ect-2(ax751)* zygotes require *par-3 and par-2*

In wild-type zygotes, *ect-2*-dependent myosin flows do not require *par-2* activity and only partially require *par-3* (Munro et al., 2004). *par-3* mutant zygotes still form anterior-directed flows, but the flows do not propagate as far towards the anterior, indicating that PAR-3 is required to amplify, but not initiate, the *ect-2*-dependent wave (Munro et al., 2004). To determine the roles of PAR-2 and PAR-3 in the formation of the late myosin wave in *ect-2(ax751)* zygotes, we depleted *par-2* by RNAi and crossed in the *par-3* mutant *par-3(it71)*. We found that NMY-2::GFP remained uniformly distributed (Fig. 3A,B) and did not form flows (Fig. 4A; see Movie 6 in the supplementary material) in *ect-2(ax751);par-2(RNAi)* zygotes (6/6). Similarly, NMY-2::GFP remained uniformly distributed (Fig. 3A)

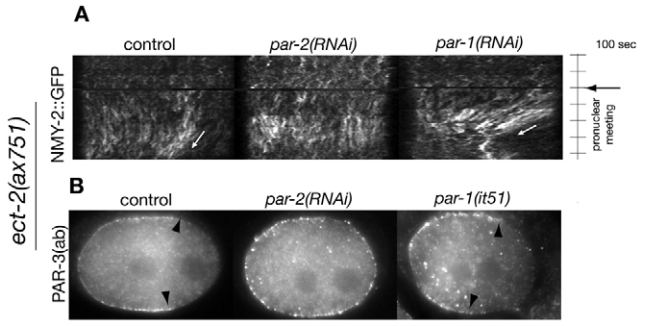

Fig. 4. *par-2*, but not *par-1*, is essential to polarize *ect-2(ax751)* zygotes. (**A**) Kymograph of *ect-2(ax751) C. elegans* zygotes expressing NMY-2::GFP and depleted for *par-2* or *par-1* by RNAi. No flows or myosin asymmetry are detected in *par-2(RNAi)*, whereas intense flows (white arrows) are present in *par-1(RNAi)* zygotes. Loss of PAR-1 has been shown to expand the anterior reach of the myosin wave also in wild type (Cuenca et al., 2003) (see Movies 6 and 9 in the supplementary material). (**B**) Staining of endogenous PAR-3 in *ect-2(ax751);par-2(RNAi)* and in *ect-2(ax751);par-1(it51)* double-mutant zygotes. Arrowheads indicate the extent of cortical PAR-3 clearing. PAR-3 becomes asymmetric in *ect-2(ax751);par-1(it51)* but not in *ect-2(ax751);par-2(RNAi).* By contrast, in *ect-2(+)* zygotes, PAR-3 initial asymmetry does not require PAR-2 (see Fig. S3 in the supplementary material) (Cuenca et al., 2003).

and did not develop strong asymmetric flows (see Fig. S3 and Movie 7 in the supplementary material) in *ect-2(ax751);par-3(it71)* zygotes (5/5). By contrast, early NMY-2::GFP flows were visible in *par-3(it71)* zygotes (see Fig. S3 in the supplementary material) (Munro et al., 2004). We conclude that, unlike in wild type, in *ect-2(ax751)* zygotes myosin flows and asymmetry are entirely dependent on PAR protein activity.

PAR-3 promotes myosin cortical localization and PAR-2 antagonizes PAR-3

Although *ect-2(ax751);par-2(RNAi)* zygotes did not polarize NMY-2::GFP, these zygotes still exhibited an increase in cortical NMY-2::GFP levels after pronuclear meeting (Fig. 3A,B; see Movie 6 in the supplementary material). This increase was observed throughout the cortex and was comparable in amplitude (1.8 fold) to that seen in the anterior cortex of *ect-2(ax751)* zygotes (Fig. 3A,B; see Movie 2 in the supplementary material). By contrast, *ect-2(ax751);par-3(it71)* zygotes exhibited only a modest 1.2-fold increase in NMY-2::GFP (Fig. 3A,B; see Movie 7 in the supplementary material). This difference could be due to a requirement for PAR-3 to boost NMY-2 cortical localization or to a requirement for PAR-2 to inhibit NMY-2 cortical localization. To distinguish between these two possibilities, we examined *ect-2(ax751);par-3(it71);par-2(RNAi)* zygotes. We found that these also exhibited only a modest (1.2 fold) increase in cortical NMY-2::GFP, identical to that seen in *ect-2(ax751);par-3(it71)* zygotes (Fig. 3A,B; see Movie 8 in the supplementary material). We conclude that PAR-3 is required to stimulate the increase in cortical NMY-2 at the onset of mitosis, and that PAR-2 resists this increase indirectly by antagonizing PAR-3.

Consistent with this result, we found that PAR-2 is essential to polarize PAR-3 in *ect-2(ax751)* zygotes. No (0/18) *ect-2(ax751);par-2(RNAi)* zygotes had asymmetric PAR-3, as compared with 12/19 *ect-2(ax751)* zygotes (Fig. 4B). In *ect-2(ax751);par-2(RNAi)* zygotes, PAR-3 was uniformly distributed even during pronuclear migration (9/9) (Fig. 4B). By contrast, in wild-type zygotes depleted of *par-2* by RNAi, PAR-3 was asymmetric in 4/4 zygotes during pronuclear migration (see Fig. S4 in the supplementary material). We conclude that in the absence of the early *ect-2*-dependent wave, PAR-2 becomes essential to polarize PAR-3.

In wild-type zygotes, PAR-1 localizes with PAR-2 on the posterior cortex (Guo and Kemphues, 1995). To determine whether PAR-1 is also required to initiate polarity in *ect-2(ax751)* zygotes, we eliminated *par-1* by RNAi or using a mutation in its kinase domain, *par-1(it51)* (Guo and Kemphues, 1995). We found that *par-1(RNAi)* did not affect NMY-2 flows in *ect-2(ax751)* zygotes (Fig. 4A; see Movie 9 in the supplementary material), and that PAR-3 was still asymmetric in *par-1(it51);ect-2(ax751)* zygotes (6/6) (Fig. 4B). We conclude that polarity initiation in *ect-2(ax751)* zygotes depends on PAR-2, but not on PAR-1.

Myosin asymmetry is not required to initiate PAR protein asymmetry

The finding that PAR-2 and PAR-3 segregate before strong myosin flows are visible in *ect-2(ax751)* zygotes raises the possibility that myosin asymmetry is not essential to initiate PAR protein asymmetry. To investigate this further, we depleted *mlc-4* by RNAi in *ect-2(ax751)*;NMY-2::GFP;mCherry::PAR-2 zygotes. As expected, *mlc-4(RNAi)* eliminated the increase in cortical NMY-2::GFP (Fig. 3A,B) and eliminated directional flows as detected by kymograph analysis (3/3) (Fig. 5A). We found that mCherry::PAR-2 still loaded on the cortex in 6/7 of *ect-2(ax751);mlc-4(RNAi)* zygotes, although in a domain smaller and more off-axis than in wild type (Fig. 5A; see Movie 10 in the supplementary material). Staining of *ect-2(ax751);mlc-4(RNAi)*;GFP::PAR-2 zygotes at pronuclear meeting revealed that in 7/8 zygotes, PAR-3 was depleted from the cortex positive for PAR-2 (see Fig. S5 in the supplementary material). To ensure that these results were not dependent on *ect-2(ax751)* or the *par-2* transgene, we repeated the analysis in NMY-2::GFP;*mlc-4(RNAi)* zygotes. Again, as expected, we observed no asymmetric flows by kymograph analysis (see Fig. S6 and Movie 11 in the supplementary material). We found, however, that PAR-3 was asymmetric in 9/14 of zygotes (post-pronuclear meeting, Fig. 5B). PAR-3 asymmetry was dependent on PAR-2 as no (0/10) NMY-2::GFP;*mlc-4(RNAi);par-2(RNAi)* zygotes had asymmetric PAR-3 (Fig. 5B). We conclude that when actomyosin contractility is severely reduced, PAR-2 can still exclude PAR-3 from the posterior cortex, although not as efficiently as is observed in wild-type zygotes.

To determine whether PAR-2 also excludes mCherry::PAR-6, we examined mCherry::PAR-6;GFP::PAR-2;*ect-2(ax751);mlc-4(RNAi)* zygotes. Surprisingly, we found that in these zygotes GFP::PAR-2 was rarely found on the cortex (1/11) and, as expected, the distribution of mCherry::PAR-6 remained uniform (10/11) (Fig. 5C). This effect requires *mlc-4(RNAi)* because mCherry::PAR-6;GFP::PAR-2;*ect-2(ax751)* localized both transgenes (Fig. 2C). We conclude that mCherry::PAR-6 requires strong myosin flows to localize and that in the absence of myosin flows, mCherry::PAR-6 (which presumably represents an increase in PAR-6 activity compared with wild type) can prevent PAR-2 from localizing to the cortex.

Polarization in *ect-2(ax751)* zygotes is sensitive to PAR protein balance

The observations above suggest that in the absence of cortical flows, polarization becomes sensitive to the balance between the levels of PAR-2 and the anterior PARs. Consistent with this, we found that expression of mCherry::PAR-6 alone in *ect-2(ax751)* zygotes was

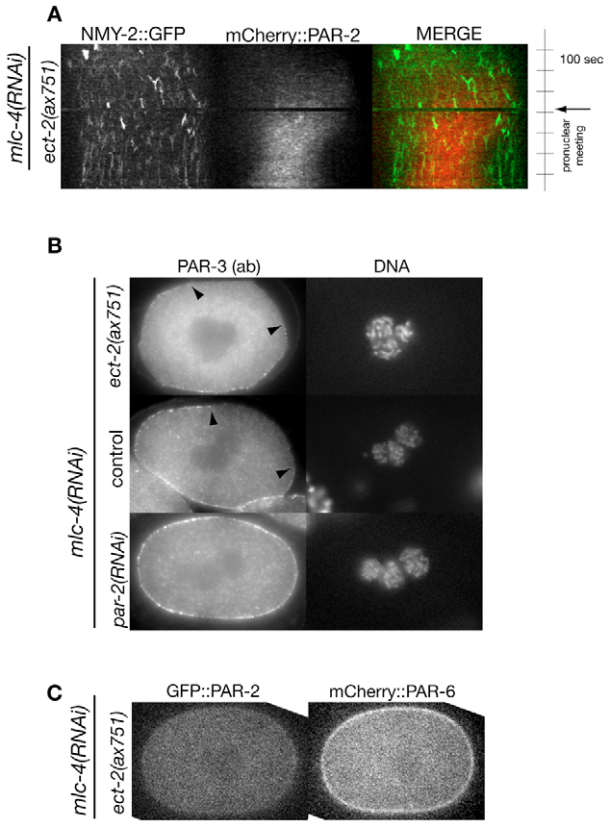

Fig. 5. Cortical PAR protein asymmetry does not require myosin asymmetry. (**A**) Kymograph of cortical sections of a *C. elegans ect-2(ax751);mlc-4(RNAi)* zygote expressing NMY-2::GFP and mCherry::PAR-2. Directed flows are not detectable even after mCherry::PAR-2 loads on the cortex. Note that PAR-2 loads laterally (instead of on the posterior pole) (see Movie 10 in the supplementary material). (**B**) Staining of endogenous PAR-3 in *mlc-4(RNAi);ect-2(ax751)*;GFP::PAR-2 zygotes or *mlc-4(RNAi)* zygotes that express no transgenes. DNA staining shows that these zygotes are all at the pronuclear meeting stage (there are three pronuclei because *mlc-4(RNAi)* blocks cytokinesis during the meiotic divisions). Arrowheads indicate the extent of cortical PAR-3 clearing. Note that PAR-3 asymmetry depends on PAR-2. (**C**) Confocal images of transverse sections of an *ect-2(ax751);mlc-4(RNAi)* zygote co-expressing GFP::PAR-2 and mCherry::PAR-6 at pronuclear meeting. GFP::PAR-2 is excluded from the cortex and mCherry::PAR-6 occupies the entire cortex.

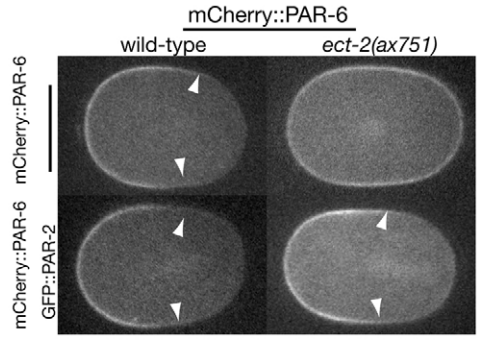

Fig. 6. *ect-2(ax751)* zygotes are sensitive to PAR protein balance. Confocal images of transverse sections of wild-type and *ect-2(ax751) C. elegans* zygotes expressing mCherry::PAR-6 alone or co-expressing mCherry::PAR-6 with GFP::PAR-2. mCherry::PAR-6 polarizes in the presence or absence of GFP::PAR-2 in the wild type, but polarizes only in the presence of GFP::PAR-2 in *ect-2(ax751)* zygotes. White arrowheads indicate the boundaries of the cortical mCherry::PAR-6 domain.

sufficient to suppress polarity. Nine out of ten *ect-2(ax751)* zygotes expressing mCherry::PAR-6 failed to localize the fusion (Fig. 6) and divided symmetrically (data not shown). Wild-type zygotes expressing the same transgene showed no defect (5/5). Remarkably, co-expression of GFP::PAR-2 and mCherry::PAR-6 rescued the polarity defect: 8/8 *ect-2(ax751)* zygotes expressing both fusions polarized both proteins and divided asymmetrically (Fig. 6). We conclude that in the absence of early cortical flows, the ability of PAR-2 to initiate polarization is sensitive to dosage, relative to that of PAR-6.

DISCUSSION

Parallel pathways for polarity initiation

Polarization of the *C. elegans* zygote involves the formation of two non-overlapping cortical domains: an anterior PAR domain containing PAR-3, PAR-6 and PKC-3, and a posterior PAR domain containing PAR-1 and PAR-2. Previous studies have identified a simple two-step pathway for PAR polarity establishment: (1) ECT-2-regulated flows sweep anterior PARs away from the cortex nearest the centrosome; and (2) cortical exclusion by PKC-3 restricts PAR-2 to the posterior cortex vacated by PKC-3 (Munro and Bowerman, 2009). Our finding that zygotes can polarize in the absence of ECT-2-regulated flows suggests the existence of a parallel pathway involving: (1) flow-independent recruitment of PAR-2 to the cortex nearest the centrosome; and (2) cortical exclusion of PAR-3 (and probably also PAR-6 and PKC-3) by PAR-2. We propose that the ECT-2- and PAR-2-initiated pathways function in parallel in wild-type zygotes to decrease the anterior PARs on the cortex nearest the sperm centrosome (Fig. 7). We also propose that in both pathways, loss of anterior PARs is amplified by a positive-feedback loop that involves PAR-3-dependent recruitment of myosin to the cortex. Loss of PAR-3 creates a local myosin minimum, which, in the context of a tensioned cortex, generates cortical flows. The flows further mobilize PAR-3 (and probably also PKC-3 and PAR-6) away from PAR-2, allowing the PAR-2 domain to expand beyond the area nearest the sperm centrosome. What ultimately stops PAR-2 domain growth is not known, but previous genetic studies have suggested the existence of an opposing negative-feedback loop involving PAR-1 and MEX-5 (Cuenca et al., 2003).

Why two pathways? The PAR-2-dependent pathway is sensitive to increases in PAR-6 levels, raising the possibility that it is not sufficiently robust to initiate polarization on its own under all conditions. PAR-2 also responds to a cue from the meiotic spindle (Tsai and Ahringer, 2007; Wallenfang and Seydoux, 2000), which is typically at the pole opposite the sperm microtubule-organizing center (MTOC). By depleting anterior PARs specifically from the cortex nearest the MTOC, ECT-2-dependent cortical flows introduce a potent bias from a single point. PAR-2 in turn ensures that the bias is irreversible by excluding anterior PARs from its own domain. We suggest that the parallel use of the ECT-2- and PAR-2-dependent pathways contributes to the robustness of the MTOC cue.

PAR-2 can sense the position of the centrosome

A key prediction of our model is that PAR-2 has the ability to recognize, and associate with, the cortex nearest the sperm centrosome. In the absence of the anterior PAR complex, PAR-2

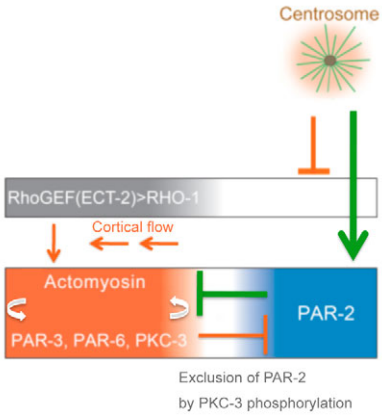

Fig. 7. Model for polarity establishment in *C. elegans* zygotes. The sperm microtubule-organizing center (MTOC) breaks symmetry using two parallel pathways. In the first pathway, an unknown cue(s) from the MTOC inactivates ECT-2 and RHO-1 on the nearby cortex, creating a cortical flow that mobilizes the anterior PARs. PAR-2, which was excluded from the cortex by PKC-3 phosphorylation, loads on the cortex vacated by the anterior PARs. In the second pathway, PAR-2 responds directly to an unknown cue from the MTOC (possibly microtubules), loads on the cortex, and excludes the anterior PARs by an unknown mechanism. In both pathways, local inactivation/displacement of anterior PARs creates cortical flows that further mobilize the anterior PARs away from the MTOC.

associates with the whole cortex with no preference for the area nearest the sperm (MTOC) (Cuenca et al., 2003). Furthermore, in the absence of flow, as in *mlc-4(RNAi)* zygotes, PAR-6 overexpression can prevent PAR-2 from loading (this study). These observations indicate that PAR-2 cortical association is inhibited by the anterior PAR complex throughout the cortex. How can PAR-2 overcome this inhibition specifically on the cortex nearest the sperm centrosome? In other work, we have found that PAR-2 binds microtubules and that this ability is required for PAR-2 to load on the cortex in the absence of cortical flows (F.M. and G.S., unpublished). One possibility is that the astral microtubules emanating from the sperm centrosome provide a binding platform for PAR-2, which raises the concentration of PAR-2 around the sperm asters. A local increase in PAR-2 could transiently overwhelm PKC-3 and allow a few molecules of PAR-2 to load on the cortex. If, once on the cortex, PAR-2 displaces PAR-3 and/or PKC-3 (see below), this initially small increase might be sufficient to tip the balance permanently in the favor of PAR-2. Although more studies will be required to understand the mechanisms involved, our studies and the study of Shelton et al. (Shelton et al., 1999) demonstrate that PAR-2 can sense the position of the sperm centrosome even in the absence of flow. We propose, therefore, that PAR-2 localization to the cortex is one of the symmetry-breaking events that signal the position of the centrosome to the cortex.

PAR-2 interferes with PAR-3-dependent recruitment of myosin to the cortex

In the presence of cortical flows, loading of PAR-2 and exclusion of the anterior PARs occur rapidly and efficiently. Previous studies have shown that cortical flows in wild-type zygotes depend both on the Rho GEF ECT-2, which is required for the formation of the dense actomyosin cables that contract the cortex during polarity initiation, and on the anterior PAR complex, which amplifies ECT-2-dependent flows (Munro et al., 2004). Elimination of the ECT-2-dependent myosin network in *ect-2(ax751)* zygotes allowed us to directly visualize the contribution of the PAR proteins to myosin dynamics. Our genetic evidence indicates that PAR-3 stimulates myosin recruitment to the cortex. We propose that, in the context of a contractile cortex, the ability of PAR-3 to recruit myosin creates a feedback loop that can amplify localized changes in PAR-3 levels. A local reduction in PAR-3 and myosin creates cortical flows, which mobilize additional PAR-3 away from the region of low PAR-3/myosin abundance. We do not yet know how PAR-3 stimulates myosin recruitment to the cortex. One possibility is that this activity depends on PAR-6 and its binding partner CDC-42 (Gotta et al., 2001), a known regulator of many actin-dependent processes (Etienne-Manneville and Hall, 2002). CDC-42 is enriched on the anterior cortex, where it is required to stabilize the actomyosin network and PAR-6 (Motegi and Sugimoto, 2006; Schonegg and Hyman, 2006). ECT-2 could also be involved. Residual ECT-2 activity in *ect-2(ax751)* and *ect-2(RNAi)* zygotes, although not sufficient to support contractility in early zygotes, could potentially contribute to myosin dynamics during mitosis. Unfortunately, this possibility cannot be investigated because *ect-2* nulls are sterile (Morita et al., 2005).

What reduces PAR-3 levels in the cortex nearest the sperm centrosome in the first place? We propose that at least two parallel mechanisms contribute to this change in wild-type zygotes. First, inactivation of ECT-2/RHO-1 flows nearest the centrosome by loss of ECT-2 (Motegi and Sugimoto, 2006) and by activation of sperm-donated CYK-4 (Jenkins et al., 2006) initiates a potent cortical flow that mobilizes PAR-3 away from the sperm centrosome. Second, loading of PAR-2 on the posterior cortex displaces PAR-3. In principle, PAR-2 could displace PAR-3 directly, by removing it from the cortex, or indirectly, by interfering with the ability of PAR-3 to recruit myosin, thus creating a cortical flow that displaces PAR-3. Our finding that PAR-2 can displace PAR-3 in at least some *mlc-4(RNAi)* zygotes suggests the former, but we do not exclude the latter as it remains possible that *mlc-4(RNAi)* zygotes retain residual myosin activity. In *Drosophila*, PAR-1 has been proposed to block PAR-3 (Bazooka – FlyBase) cortical localization by direct phosphorylation (Benton et al., 2002). It is unlikely that PAR-1 plays a similar role here because PAR-1, unlike PAR-2, is not required for PAR-3 or myosin asymmetry in *ect-2(ax751)* zygotes.

Direct PAR-2 homologs have not been identified in other organisms, but the tumor suppressor Lethal giant larvae (LGL) might serve an analogous role (Goldstein and Macara, 2007). In epithelial cells, LGL localizes to the basolateral cortex, opposite aPKC, PAR-3 and PAR-6 on the apical cortex. LGL is directly phosphorylated by aPKC and this phosphorylation excludes LGL from the apical cortex. LGL in turn competes with PAR-3 in forming a complex with PAR-6 and aPKC, and overexpression of LGL can displace PAR-6 from the apical cortex (Hutterer et al., 2004; Goldstein and Macara, 2007). Recently, *Drosophila* LGL [L(2)GL] was reported to inhibit aPKC kinase activity in vitro, possibly by acting as a competitive inhibitor (Atwood and Prehoda, 2009). An LGL homolog exists in *C. elegans* and has been shown to function redundantly with PAR-2 in polarity maintenance (Alex Beatty and Ken Kemphues, personal communication). It will be interesting to determine whether LGL also functions with PAR-2 in symmetry breaking.

Acknowledgements
We thank Julie Ahringer for the PAR-2 antibody and Erik Griffin for mCherry::PAR-6. Some strains and antibodies were provided by the NIH-funded Caenorhabditis Genetics Center and the Developmental Studies

Hybridoma Bank. This work was supported by National Institutes of Health grant HD37047 (to G.S.), and G.S. is an investigator of the Howard Hughes Medical Institute. Deposited in PMC for release after 6 months.

Competing interests statement
The authors declare no competing financial interests.

Supplementary material
Supplementary material for this article is available at
http://dev.biologists.org/lookup/suppl/doi:10.1242/dev.045823/-/DC1

References

Atwood, S. X. and Prehoda, K. E. (2009). aPKC phosphorylates Miranda to polarize fate determinants during neuroblast asymmetric cell division. *Curr. Biol.* **19**, 723-729.
Benton, R., Palacios, I. M. and St Johnston, D. (2002). Drosophila 14-3-3/PAR-5 is an essential mediator of PAR-1 function in axis formation. *Dev. Cell* **3**, 659-671.
Brenner, S. (1974). The genetics of Caenorhabditis elegans. *Genetics* **77**, 71-94.
Cheeks, R. J., Canman, J. C., Gabriel, W. N., Meyer, N., Strome, S. and Goldstein, B. (2004). C. elegans PAR proteins function by mobilizing and stabilizing asymmetrically localized protein complexes. *Curr. Biol.* **14**, 851-862.
Cuenca, A. A., Schetter, A., Aceto, D., Kemphues, K. and Seydoux, G. (2003). Polarization of the C. elegans zygote proceeds via distinct establishment and maintenance phases. *Development* **130**, 1255-1265.
Davis, M. W., Hammarlund, M., Harrach, T., Hullett, P., Olsen, S. and Jorgensen, E. M. (2005). Rapid single nucleotide polymorphism mapping in C. elegans. *BMC Genomics* **6**, 118.
Dechant, R. and Glotzer, M. (2003). Centrosome separation and central spindle assembly act in redundant pathways that regulate microtubule density and trigger cleavage furrow formation. *Dev. Cell* **4**, 333-344.
Encalada, S. E., Martin, P. R., Phillips, J. B., Lyczak, R., Hamill, D. R., Swan, K. A. and Bowerman, B. (2000). DNA replication defects delay cell division and disrupt cell polarity in early Caenorhabditis elegans embryos. *Dev. Biol.* **228**, 225-238.
Etienne-Manneville, S. and Hall, A. (2002). Rho GTPases in cell biology. *Nature* **420**, 629-635.
Goldstein, B. and Macara, I. G. (2007). The PAR proteins: fundamental players in animal cell polarization. *Dev. Cell* **13**, 609-622.
Gotta, M., Abraham, M. C. and Ahringer, J. (2001). CDC-42 controls early cell polarity and spindle orientation in C. elegans. *Curr. Biol.* **11**, 482-488.
Gotta, M., Dong, Y., Peterson, Y. K., Lanier, S. M. and Ahringer, J. (2003). Asymmetrically distributed C. elegans homologs of AGS3/PINS control spindle position in the early embryo. *Curr. Biol.* **13**, 1029-1037.
Guo, S. and Kemphues, K. J. (1995). par-1, a gene required for establishing polarity in C. elegans embryos, encodes a putative Ser/Thr kinase that is asymmetrically distributed. *Cell* **81**, 611-620.
Guo, S. and Kemphues, K. J. (1996). Molecular genetics of asymmetric cleavage in the early Caenorhabditis elegans embryo. *Curr. Opin. Genet. Dev.* **6**, 408-415.
Hao, Y., Boyd, L. and Seydoux, G. (2006). Stabilization of cell polarity by the C. elegans RING protein PAR-2. *Dev. Cell* **10**, 199-208.
Hurov, J. B., Watkins, J. L. and Piwnica-Worms, H. (2004). Atypical PKC phosphorylates PAR-1 kinases to regulate localization and activity. *Curr. Biol.* **14**, 736-741.
Hutterer, A., Betschinger, J., Petronczki, M. and Knoblich, J. A. (2004). Sequential roles of Cdc42, Par-6, aPKC, and Lgl in the establishment of epithelial polarity during Drosophila embryogenesis. *Dev. Cell* **6**, 845-854.
Ikebe, M. and Hartshorne, D. J. (1985). Phosphorylation of smooth muscle myosin at two distinct sites by myosin light chain kinase. *J. Biol. Chem.* **260**, 10027-10031.
Jenkins, N., Saam, J. R. and Mango, S. E. (2006). CYK-4/GAP provides a localized cue to initiate anteroposterior polarity upon fertilization. *Science* **313**, 1298-1301.
Kamath, R. S., Fraser, A. G., Dong, Y., Poulin, G., Durbin, R., Gotta, M., Kanapin, A., Le Bot, N., Moreno, S., Sohrmann, M. et al. (2003). Systematic functional analysis of the Caenorhabditis elegans genome using RNAi. *Nature* **421**, 231-237.
Kemphues, K. (2000). PARsing embryonic polarity. *Cell* **101**, 345-348.
Maeda, I., Kohara, Y., Yamamoto, M. and Sugimoto, A. (2001). Large-scale analysis of gene function in Caenorhabditis elegans by high-throughput RNAi. *Curr. Biol.* **11**, 171-176.
Morita, K., Hirono, K. and Han, M. (2005). The Caenorhabditis elegans ect-2 RhoGEF gene regulates cytokinesis and migration of epidermal P cells. *EMBO Rep.* **6**, 1163-1168.
Motegi, F. and Sugimoto, A. (2006). Sequential functioning of the ECT-2 RhoGEF, RHO-1 and CDC-42 establishes cell polarity in Caenorhabditis elegans embryos. *Nat. Cell Biol.* **8**, 978-985.
Munro, E. and Bowerman, B. (2009). Cellular symmetry breaking during Caenorhabditis elegans development. *Cold Spring Harbor Perspect. Biol.* **1**, a003400.
Munro, E., Nance, J. and Priess, J. R. (2004). Cortical flows powered by asymmetrical contraction transport PAR proteins to establish and maintain anterior-posterior polarity in the early C. elegans embryo. *Dev. Cell* **7**, 413-424.
Nance, J., Munro, E. M. and Priess, J. R. (2003). C. elegans PAR-3 and PAR-6 are required for apicobasal asymmetries associated with cell adhesion and gastrulation. *Development* **130**, 5339-5350.
Riento, K. and Ridley, A. J. (2003). Rocks: multifunctional kinases in cell behaviour. *Nat. Rev. Mol. Cell Biol.* **4**, 446-456.
Schonegg, S. and Hyman, A. A. (2006). CDC-42 and RHO-1 coordinate acto-myosin contractility and PAR protein localization during polarity establishment in C. elegans embryos. *Development* **133**, 3507-3516.
Shaham, S. (2006). Methods in cell biology. *WormBook* (ed. The C. elegans Research Community). doi/10.1895/wormbook.1.49.1, http://www.wormbook.org.
Shelton, C. A., Carter, J. C., Ellis, G. C. and Bowerman, B. (1999). The nonmuscle myosin regulatory light chain gene mlc-4 is required for cytokinesis, anterior-posterior polarity, and body morphology during Caenorhabditis elegans embryogenesis. *J. Cell Biol.* **146**, 439-451.
Tenenhaus, C., Schubert, C. and Seydoux, G. (1998). Genetic requirements for PIE-1 localization and inhibition of gene expression in the embryonic germ lineage of Caenorhabditis elegans. *Dev. Biol.* **200**, 212-224.
Timmons, L. and Fire, A. (1998). Specific interference by ingested dsRNA. *Nature* **395**, 854.
Tsai, M. C. and Ahringer, J. (2007). Microtubules are involved in anterior-posterior axis formation in C. elegans embryos. *J. Cell Biol.* **179**, 397-402.
Wallenfang, M. R. and Seydoux, G. (2000). Polarization of the anterior-posterior axis of C. elegans is a microtubule-directed process. *Nature* **408**, 89-92.